THE JOURNAL OF BIOLOGICAL CHEMISTRY VOL. 288, NO. 40, pp. 29105–29114, October 4, 2013

FRAX597, a Small Molecule Inhibitor of the p21-activated Kinases, Inhibits Tumorigenesis of Neurofibromatosis Type 2 (NF2)-associated Schwannomas*

Received for publication, August 15, 2013 Published, JBC Papers in Press, August 19, 2013, DOI 10.1074/jbc.M113.510933

Silvia Licciulli[‡1], Jasna Maksimoska[§1], Chun Zhou[¶1], Scott Troutman[‡1], Smitha Kota[‡], Qin Liu[¶], Sergio Duron[‖], David Campbell[‖], Jonathan Chernoff[**], Jeffrey Field[‡‡], Ronen Marmorstein[§], and Joseph L. Kissil[‡2]

From the [‡]Department of Cancer Biology, The Scripps Research Institute, Jupiter, Florida 33458, [§]Gene Expression and Regulation and [¶]Molecular Oncogenesis Programs, The Wistar Institute, Philadelphia, Pennsylvania 19104, [‖]Afraxis, Inc., San Diego, California 92037, the [**]Cancer Biology Program, Fox Chase Cancer Center, Philadelphia, Pennsylvania 19111, and the [‡‡]Department of Pharmacology, Perelman School of Medicine, University of Pennsylvania, Philadelphia, Pennsylvania 19104

Background: The PAKs are effectors of Rac/cdc42.
Results: Identification of a pyridopyrimidinone, as a potent inhibitor of the group I PAKs that shows anti-tumor activity *in vivo*.
Conclusion: A pyridopyrimidinone provides a scaffold for development of high specificity group I PAK inhibitors.
Significance: Identification class of orally available ATP-competitive Group I PAK inhibitors with significant potential for the treatment of NF2.

The p21-activated kinases (PAKs) are immediate downstream effectors of the Rac/Cdc42 small G-proteins and implicated in promoting tumorigenesis in various types of cancer including breast and lung carcinomas. Recent studies have established a requirement for the PAKs in the pathogenesis of Neurofibromatosis type 2 (NF2), a dominantly inherited cancer disorder caused by mutations at the *NF2* gene locus. Merlin, the protein product of the *NF2* gene, has been shown to negatively regulate signaling through the PAKs and the tumor suppressive functions of Merlin are mediated, at least in part, through inhibition of the PAKs. Knockdown of PAK1 and PAK2 expression, through RNAi-based approaches, impairs the proliferation of NF2-null schwannoma cells in culture and inhibits their ability to form tumors *in vivo*. These data implicate the PAKs as potential therapeutic targets. High-throughput screening of a library of small molecules combined with a structure-activity relationship approach resulted in the identification of FRAX597, a small-molecule pyridopyrimidinone, as a potent inhibitor of the group I PAKs. Crystallographic characterization of the FRAX597/PAK1 complex identifies a phenyl ring that traverses the gatekeeper residue and positions the thiazole in the back cavity of the ATP binding site, a site rarely targeted by kinase inhibitors. FRAX597 inhibits the proliferation of NF2-deficient schwannoma cells in culture and displayed potent anti-tumor activity *in vivo*, impairing schwannoma development in an orthotopic model of NF2. These studies identify a novel class of orally available ATP-competitive Group I PAK inhibitors with significant potential for the treatment of NF2 and other cancers.

The p21-activated kinases (PAKs)[3] form a protein family of serine/threonine kinases, divided into two sub groups, I and II. Group I PAKs consists of three members - PAK1, PAK2, and PAK3 that share 93–95% sequence identity within the kinase domain and are similarly regulated by Rac/Cdc42-GTP binding (1). The Rac and Cdc42 proteins are members of the Rho family of small G-proteins and mediate several signaling pathways that regulate cellular proliferation, cytoskeleton reorganization, and gene expression (2, 3). As immediate downstream effectors of Rac/Cdc42 and given the major roles these small G-proteins play in tumorigenesis, the PAKs have been implicated in multiple types of cancer including breast and lung carcinomas and neurofibromatosis (4, 5).

PAK1 has been reported to be widely overexpressed and/or hyperactivated in various types of benign and malignant cancers (6). PAK1 expression is up-regulated in 40–50% of primary breast cancers (7, 8). Expression of a constitutively active PAK1 mutant (CA-PAK1) increases cell motility, anchorage-independent growth, and invasiveness of breast cancer cells and leads to dissemination of metastatic mammary tumors and other types of breast lesions in transgenic mouse models (9–11). Conversely, inhibition of PAK1 function suppresses cellular motility and invasiveness of breast cancer cell lines and inhibits pre-malignant progression in a three-dimensional culture model of breast cancer (10, 12–15). In squamous non-small cell lung cancer (NSCLC), PAK1 expression is elevated in 64% of cases and is required for the proliferation of squamous NSCLC cells and for tumor growth *in vivo* (8).

* This work was supported, in whole or in part, by National Institutes of Health Grants CA124495 (to J. K.), CA114046 (to R. M.), and CA148805 (to J. C.) and from the American Cancer Society RSG-10-018-01-CDD (to J. K.). Work in the J. L. K.'s laboratory was also supported by Afraxis and the Children's Tumor Foundation.

The atomic coordinates and structure factors (code 4EQC) have been deposited in the Protein Data Bank (http://wwpdb.org/).

[1] These authors contributed equally to this manuscript.

[2] To whom correspondence should be addressed: Department of Cancer Biology. The Scripps Research Institute, Jupiter, Florida 33458. E-mail: jkissil@scripps.edu.

[3] The abbreviations used are: PAK, p21-activated kinase; NF2, neurofibromatosis type 2; NSCLC, non-small cell lung cancer; BMMC, bone marrow-derived mast cell; LOH, loss-of-heterozygosity; PI, propidium iodide.

The PAKs play critical roles in neurofibromatosis types 1 (NF1) and 2 (NF2). NF1 and NF2 are dominantly inherited cancer disorders that develop mostly benign nerve sheath tumors of the peripheral nerves (16). NF1 is quite common with a birth incidence of 1 in 3,000 and is caused by mutations of the *NF1* tumor suppressor gene that encodes a Ras GTPase-activating protein (GAP) named Neurofibromin. Deletion/inactivation of Neurofibromin leads to increased levels of activated GTP-bound Ras, which activates multiple oncogenic signaling cascades, including the MAPK and PI3K pathways. Previous studies have shown that dominant-negative PAK1 mutants efficiently block Ras transformation in both transformed Schwann cells and malignant peripheral nerve sheath tumor cells by interfering with the activation of the MAPK cascade (17). More recently, PAK1 has been shown to play a critical role in regulating the NF1 tumor microenvironment. Previous studies have established that *Nf1* heterozygosity in the tumor microenvironment, particularly in bone marrow-derived mast cells (BMMCs), is required to induce neurofibroma progression (18–20). Genetic approaches involving the crossing of $Pak1^{-/-}$ mice with $Nf1^{+/-}$ mice have demonstrated that loss of *Pak1* reversed MAPK-mediated hyperproliferation and p38-regulated increased migration of *Nf1* haploinsufficient BMMCs in culture and corrected dermal accumulation of $Nf1^{+/-}$ mast cells *in vivo*, to levels found in wild-type mice (21).

NF2 is a dominantly inherited autosomal disease (affecting 1 in 30,000) attributed to the loss-of-heterozygosity (LOH) of the *NF2* gene. Merlin, the protein encoded by the NF2 gene, has been implicated in the regulation of a number of signaling pathways, including those regulated by Rac1, Ras/MAPK, mTOR, and Hpo (22). Several lines of evidence indicate that merlin functions as an inhibitor of Rac signaling. First, in NF2 patients, loss of Merlin is associated with elevated levels of Rac-GTP accompanied by abnormal PAK1 activation and the ablation of merlin in mouse embryo fibroblasts (MEFs) leads to PAK1 activation (23–26). Conversely, merlin overexpression in Schwann cells suppresses PAK1 activity and prevents PAK1 and PAK2 activation by Rac through competing with Rac-GTP for PAK binding (27–31). Importantly, previous work has established the PAKs as *bona fide* targets for inhibition in NF2. Use of RNAi approaches or specific peptide inhibitors to knockdown expression or inhibit the function of the group 1 PAKs, respectively, has demonstrated that the PAKs are required for cell transformation and tumorigenesis, subsequent to NF2 loss of function (25, 32). More recently a specific PAK inhibitor, IPA-3, was shown to block PAK2 phosphorylation at Ser-192/197, which antagonizes PAK-Pix interactions and reduces cell spreading and adhesion (33).

Given the data implicating the group I Paks as targets in NF2 and other types of cancers, we set out to identify PAK inhibitors to be developed as therapeutic agents. We describe the identification of a potent new small-molecule PAK inhibitor, FRAX597, characterize the molecular basis underlying the selectivity of this inhibitor and its anti-proliferative activities toward Nf2-null Schwann cells in culture and Nf2-associated schwannomas *in vivo*.

EXPERIMENTAL PROCEDURES

Cell Culture Conditions—SC4 cells are a gift from Dr. Marco Giovannini (House Ear Institute) and tested by PCR to confirm the presence of the Nf2 knock-out alleles. Cells were grown in low-glucose DME, 10% fetal calf serum, 1× non-essential amino acids and 100 IU/ml penicillin-streptomycin. Transfections were performed with Lipofectamine2000 (Invitrogen), following manufacturer's instructions.

Determination of Enzyme IC_{50} Values—IC_{50} values were determined using a 10 concentration point, non-radioactive, functional assay that employs a fluorescence-based, coupled-enzyme format, according to the manufacturer's protocol (Z′-LYTE® biochemical assay, Invitrogen). Kinase selectivity was determined using both the Z′-LYTE® and Adapta® kinase assay format provided by Invitrogen.

Western Blot Analysis—Protein extracts were prepared with RIPA lysis buffer (50 mM Tris-HCl, pH 7.5, 1% Nonidet P-40, 0.25% sodium deoxycholate, 150 mM NaCl, 1 mM EGTA, 1 mM sodium orthovanadate, and 1 mM NaF). The following antibodies were used according to manufactures' instructions: PAK1 (N-20 Santa Cruz Biotechnology), phospho-PAK1 (2606), YES1 (3201), TEK (7403), and CSF1R (3152) all from Cell Signaling, RET (ab134100 Abcam), α-tubulin (AC42 Sigma), and β-actin (AC40 Sigma).

Proliferation and Cell Cycle Assays—30,000 cells/well were plated in 12-well dishes in triplicate. Cell growth media with or without FRAX597 was replaced daily. At indicated time points, cells from individual wells were trypsinized and counted using a Coulter counter (Z1 series, Beckman Coulter). Statistical analysis was performed using a Student's *t* test. For cell cycle analysis, cells were harvested, washed once with PBS and fixed in cold 70% ethanol. Fixed cells were resuspended in propidium iodide (PI) buffer (50 μg/ml PI, 250 mg/ml RNase A in PBS) and incubated overnight at 4 °C in the dark. Cell cycle distribution was evaluated using Coulter Epics XL flow cytometer (Beckman). Data were analyzed using WinMDI software.

In Vivo Tumor Models and Imaging—All animal experiments were approved by the Wistar Institutional Animal Care and Use Committee and performed in accordance with relevant institutional and national guidelines.

$Nf2^{-/-}$ SC4 Schwann cells were transduced by lentiviruses carrying pLuc-mCherry and sorted by FACS. 5×10^4 cells were transplanted into the sciatic nerve sheath of NOD/SCID mice (8 weeks of age) by intraneural injection. Tumor progression was monitored weekly by bioluminescence imaging (BLI) according to the manufacturer's instructions on an IVIS-200 system (Xenogen, San Francisco, CA).

Statistical Analysis—To assess the anti-tumor activity of FRAX597 *in vivo*, the natural log-transformed flux readings were used to reflect tumor growth. The trends of tumor growth over time (followed up by days) were examined between control and treatment groups using a mixed-effect model with the random effect at the mouse level. A linear function in days was determined to provide the best fit without random slope on follow-up days. A likelihood ratio testing nested models (with *versus* without the interaction term of group and time) was used to examine if trends are significantly different overall between

groups. The tumor weights were first examined by a Shapiro-Wilk test to assess data normality and a Variance ratio test was used to examine the equality of variances between two groups. The differences between the control and experimental cohorts were analyzed by a *t* test with equal variances. Statistical analyses were performed using Stata 12.0 (StataCorp LP).

Recombinant PAK1 Protein Expression, Purification, and Mutagenesis—The DNA encoding the native kinase domain of PAK1 (residues 249 to 545) was subcloned into the pFastBac HTc expression vector. PAK1 V342 substitution mutants (V342F or V342Y) were generated by site-directed mutagenesis according to the manufacturer's protocol (Stratagene, La Jolla, CA). Recombinant protein was expressed in Sf21 cells, and cells were harvested and lysed by sonication in 50 mM HEPES pH 7.0, 500 mM NaCl, and 5 mM DTT (lysis buffer). The lysate was cleared by centrifugation and applied to a Ni-NTA affinity column. The protein was eluted from the column with increasing concentration of imidazole in lysis buffer (20 mM to 250 mM). Collected protein was treated overnight with TEV protease to cleave the His_6 tag. The protein was further purified by passage through a HiTrapQ column and a size-exclusion Superdex 200 column equilibrated with 20 mM Tris pH 8.0, 125 mM NaCl. Purified protein was concentrated to 1.2 mg/ml and frozen for storage. FRAX597 inhibitor potencies against wild type and V342 mutant proteins were measured using the KinaseGlo Assay (Promega) according to the manufacturer's protocol. Experiments were done in duplicate in the presence of 20 nM PAK1 and 1 μM ATP.

PAK1 Structure Determination—The PAK1 kinase domain (residues 249 to 545, mutation K299R) was cloned into a pET-TOPO vector with an N-terminal 6-His tag and expressed in BL21(DE3) *Escherichia coli* cells. Cells were grown at 37 °C until they reached an A_{600} of 0.6, and protein expression was induced by adding 1 mM IPTG and carried on for 6 h at 28 °C. Protein was purified from harvested cells as described above. Purified protein was concentrated to 9 mg/ml in a buffer containing 20 mM Tris pH 8.0, 125 mM NaCl and used for crystallization.

Crystals of apo-PAK1 were obtained using hanging drop vapor diffusion by mixing 1 μl of PAK1 (9 mg/ml) with 1 μl of crystallization solution (0.1 M HEPES pH 7.0, 1 M NaCl, 25% PEG 3350, 10 mM DTT) at 4 °C. Crystals were subjected to soaking with 1 mM FRAX597 inhibitor overnight. Crystals were cryoprotected, flash frozen in liquid nitrogen, and yielded x-ray diffraction to 2 Å on a Rigaku MicroMax-007HF x-ray generator equipped with Saturn 944+ detector. Collected data were integrated and scaled using the program HKL2000 (34).

The PAK1 inhibitor complex structure was determined by molecular replacement using the program PHASER with the structure of PAK1 (249–545, K299R) in complex with Λ-FL172 (PDB code 3FXZ) as a search model (35) with the Λ-FL172 inhibitor removed from the search model. Iterative cycles of refinement and manual rebuilding of the initial model were performed using the programs REFMAC5 (36) and COOT (37), respectively. The inhibitor models were manually fitted into the calculated F_o-F_c map. The validity of each step of refinement and rebuilding was monitored by the R_{work} and R_{free} (data not shown).

RESULTS

Discovery and Characterization of FRAX597 as a Group I PAK Inhibitor—The small molecule pyridopyrimidinone inhibitor FRAX597 was designed through a traditional structure-activity relationship (SAR) approach starting from a distinct chemical series identified from a high throughput screen (HTS) of a 12,000 member kinase-focused library against PAK1 (Fig. 1). Hits exhibiting >50% inhibition at 10 μM were prioritized, followed up with a 7 point dose response that led to the identification of a class of unsubstituted pyridopyrimidinones that demonstrated moderate inhibition of group 1 and group 2 PAK. Standard medicinal chemistry SAR evaluations of the HTS hit FRAX019 identified that 6-substitution with an aryl group on the pyridopyrimidinone core, shown in FRAX414, improved group 1 PAK potency while also improving group 2 PAK selectivity (Fig. 1*A*). Further optimization of the 6-aryl-substituted pyridopyrimidinones led to the discovery of the molecule FRAX597 (Fig. 1*B*).

FRAX597 was determined to be a potent, ATP-competitive inhibitor of group I PAKs (PAK 1–3), with biochemical IC_{50} values as follows: PAK1 IC_{50} = 8 nM, PAK2 IC_{50} = 13 nM, PAK3 IC_{50} = 19 nM. The IC_{50} toward PAK4, a member of group II PAKs was >10 μM (Fig. 1*C*). To characterize the specificity of FRAX597, the inhibitory capacity of the compound was profiled against a representative panel of recombinant kinase domains (106 of 518 known human kinases), using an assay that monitors phosphorylation of a peptide substrate (Invitrogen Z′-LYTE® biochemical assay). At a concentration of 100 nM FRAX597 displayed a significant (>80% inhibition) inhibitory capacity toward YES1 (87%), RET (82%), CSF1R (91%), TEK (87%), PAK1 (82%), and PAK2 (93%). FRAX597 displayed minimal inhibitory activity toward the group II PAKs: PAK4 (0%), PAK6 (23%), and PAK7 (8%) (data not shown). To determine the cellular IC_{50} values for FRAX597, SC4 cells (Nf2-null Schwann cells) were treated with an escalating dose of FRAX597. PAK1 activation requires an autophosphorylation step and thus the activity of PAK1 was determined by Western blot analysis using an antibody against phospho(Ser-144)-PAK1. These studies establish an approximate IC_{50} of 70 nM for FRAX597 in culture (Fig. 1*D*).

Structure of PAK1 in Complex with FRAX597—To identify the molecular basis for FRAX597 inhibition of PAK1, we determined the x-ray crystal structure of the PAK1/FRAX597 complex (PDB ID 4EQC and RCSB 071940). The 2-Å resolution structure of PAK1 in complex with FRAX597 reveals a characteristic protein kinase fold containing smaller N-terminal and larger C-terminal lobes connected by a hinge region, with the inhibitor occupying the ATP binding site as expected (Fig. 2*A*). Clear and unambiguous F_o-F_c difference electron density confirms the position and orientation of the inhibitor in the ATP binding pocket (Fig. 2*B*).

The pyrido[2,3-d]pyrimidin-7-one moiety of FRAX597 is positioned in a fashion similar to the adenine base of ATP and dictates the orientation of the entire compound. Although the ring system forms two hydrogen bonds with the hinge region, its precise hydrogen-bonding pattern is different than ATP. While the N3 nitrogen of the pyrido[2,3-d]pyrimidin-7-one

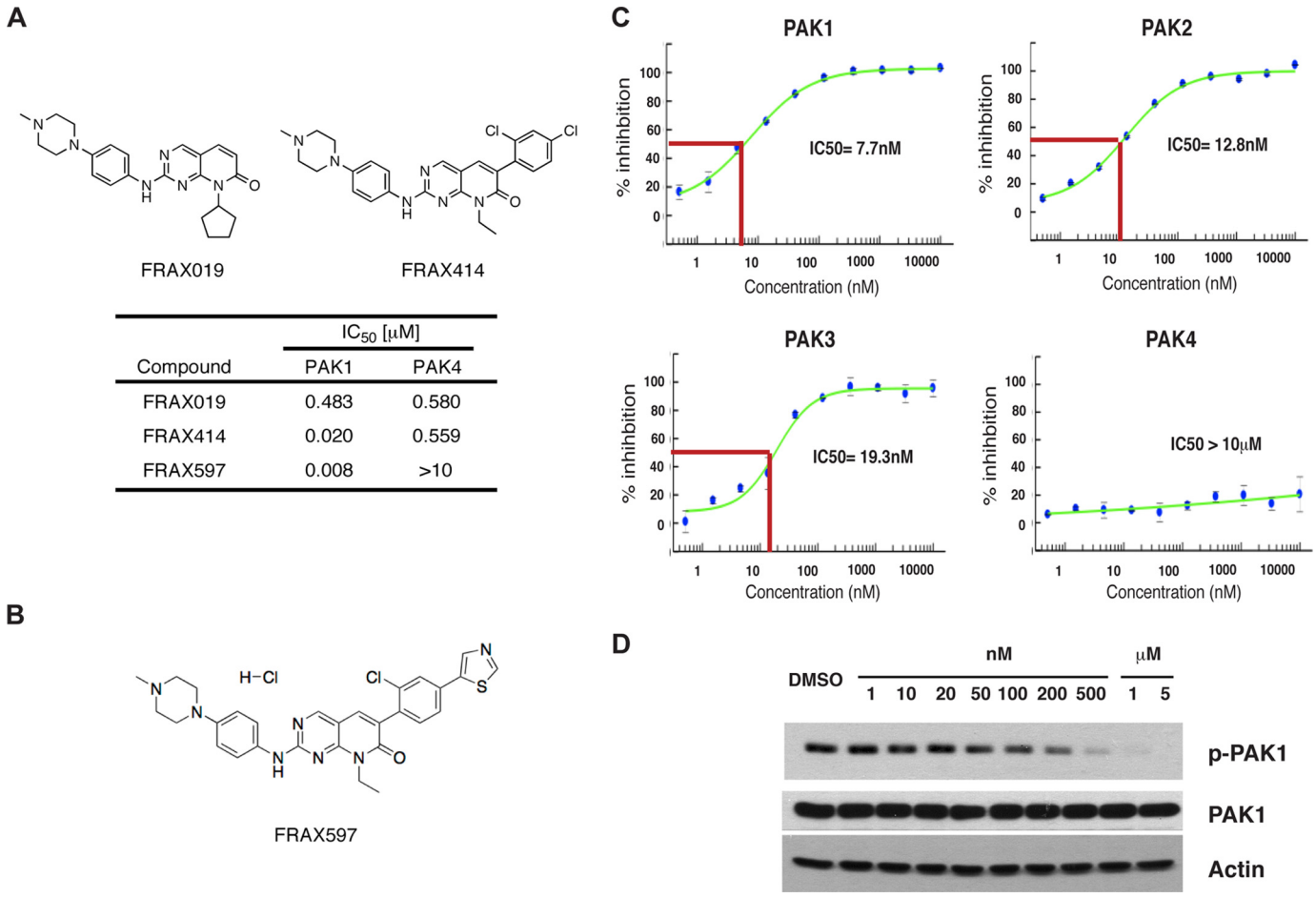

Compound	IC_{50} [μM] PAK1	PAK4
FRAX019	0.483	0.580
FRAX414	0.020	0.559
FRAX597	0.008	>10

FIGURE 1. **Characterization of FRAX597.** *A*, chemical structures and IC_{50} of FRAX019 and FRAX414. *B*, chemical structure of FRAX597. *C*, inhibition profiles for FRAX597 against group I PAKs1–3 and group II PAK4. Each of the 10 concentration points was done in duplicate. *D*, Western blot analysis of FRAX597 inhibition of PAK1 autophosphorylation (p-PAK1). SC4 cells were treated in culture for 2 h at the indicated FRAX597 concentrations and then extracted for protein. Actin was used as a loading control.

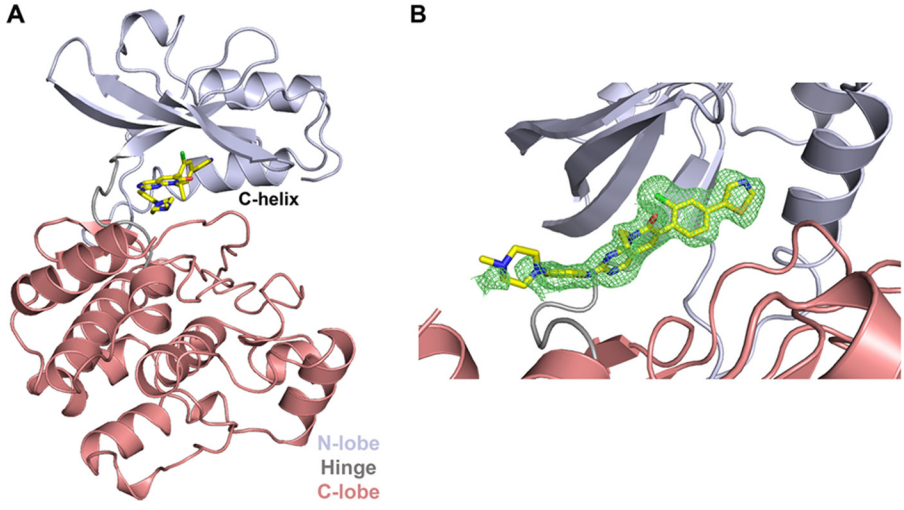

FIGURE 2. **Structure of the PAK1/FRAX597 complex.** *A*, overall structure of PAK1 with FRAX597 bound in the active site. The N-terminal lobe is shown in *light gray*, the hinge region is shown in *dark gray*, and the C-terminal lobe is shown in *salmon*. The C-helix is labeled. *B*, electron density corresponding to FRAX597. A Fo−Fc electron density map is shown in *green* and contoured at 2 σ as calculated before building the inhibitor model.

ring hydrogen bonds to the amide nitrogen of Leu-347, the other hydrogen bond is not to Glu-345, as seen in ATP and ATP analogs, but is formed between the NH group of the phenylamino moiety to the carbonyl oxygen of Leu-347 (Fig. 3*A*). The entire ring system establishes one additional hydrogen bond between the carbonyl oxygen at position 7 of the inhibitor and Arg-299 of the protein, and presumably Lys-299 of the native protein (a K299R mutation was introduced into the recombi-

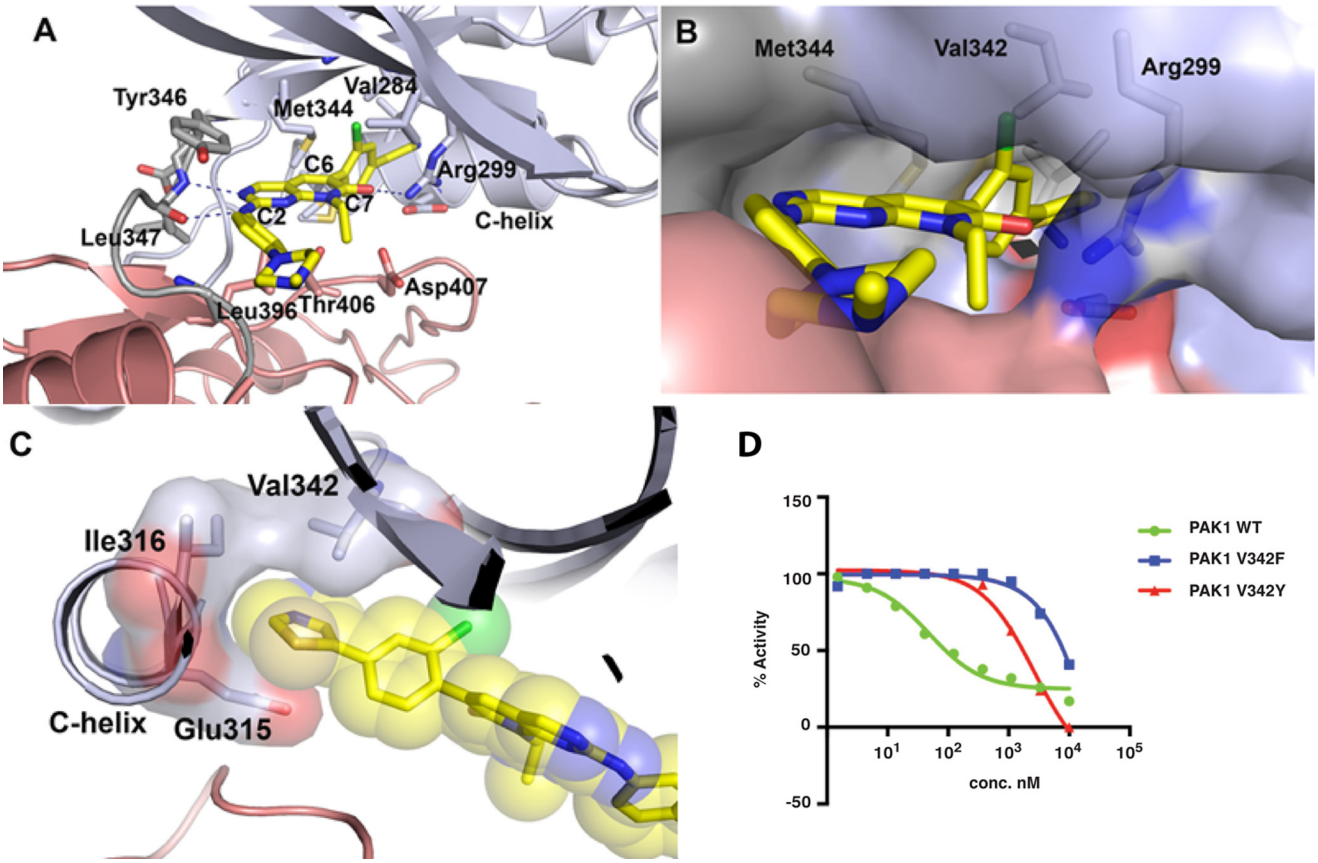

FIGURE 3. **Detailed view of the interactions of FRAX597 within the PAK1 active site.** *A*, view of the PAK1 active site in complex with FRAX597. Residues that form the binding pocket for the inhibitor are labeled. Numbering for important carbon atoms of FRAX597 is shown. *B*, surface view of the gatekeeper residue and the back cavity of the ATP binding site. Residues involved in inhibitor binding are labeled. *C*, Van der Waals sphere representation of the inhibitor and surface representation of the residues forming the back cavity of the ATP binding site. *D*, inhibition profiles for FRAX597 against wild type PAK1 and Val342 mutants. Each of the 10 concentration points was done in duplicate at 1 μM ATP and 20 nM PAK1.

nant protein to facilitate the preparation of homogeneous inactive enzyme). The pyrido[2,3-d]pyrimidin-7-one ring also establishes extensive van der Waals interactions with the protein. Ile-276, Val-284, and Ala-297 from the N-terminal domain, Leu-396, Thr-406, and Asp-407 from the C-terminal domain, and Tyr-346 and Leu-347 from the hinge region form a hydrophobic pocket that nicely accommodates the pyrido-[2,3-d]pyrimidin-7-one moiety and phenylamino substituent at position 2 of the inhibitor (Fig. 3*A*).

The C6 substituent of the inhibitor, 2-chloro-4-(thiazol-5-yl)phenyl, penetrates deeply into the back cavity of the ATP binding site. The aromatic ring of the chlorophenyl moiety is nicely placed between the hydrophobic side chains of the Met-344 gatekeeper residue and the aliphatic carbons of Arg-299 (Fig. 3*B*), allowing the thiazole group to protrude into the back cavity of the ATP binding site formed by Glu-315, Ile-316, and Val-342 (Fig. 3*C*).

In contrast to the rest of the inhibitor that makes extensive interactions with the protein, the methyl-piperazine ligand points out of the ATP binding pocket toward where the protein substrate would bind. The entire group is solvent exposed with no apparent interactions with the protein (Figs. 2*A* and 3*A*). This is in agreement with the observation that very weak electron density is observed for this group in the structure (Fig. 2*B*), suggesting possible flexibility of this region of the inhibitor when bound to PAK1 (Fig. 3*A*).

Structural Basis for FRAX597 Potency and Selectivity toward Group I PAKs—To compare the binding mode of FRAX597 to other potent PAK1 inhibitors, we superimposed the structure of the PAK1/FRAX597 complex with PAK1 bound to two organometallic inhibitors, FL172 (38) and Ru-phthalimide (39). Although all three inhibitors target the ATP binding site and mimic ATP binding, there is one striking difference; the 2-chloro-4-(thiazol-5-yl)phenyl moiety of FRAX597 occupies a part of the active site that is not sampled by the other inhibitors (Fig. 4*A*). Specifically, the 2-chloro-phenyl ring very efficiently traverses the Met-344 gatekeeper residue, and positions the thiazole in the back cavity of the ATP binding site (Fig. 3*B*).

FRAX597 shows significant isoform selectivity within the PAK family, targeting only group I PAKs. To understand the molecular basis for this specificity, we superimposed the PAK1/FRAX597 structure with the structure of PAK4 in complex with CGP74514A, a selective inhibitor of group 2 PAKs (Fig. 4*B*) (40). This superposition reveals that although the architecture of the ATP binding pockets shows similarities between the two kinases, the back cavity of PAK4 is much more constricted than in PAK1. This increased constriction in PAK4 is largely mediated by gatekeeper residue Met-395 and Lys-350 of PAK4 which are in distinctly different conformations than the corresponding residues in PAK1. This would result in a steric clash in PAK4 when a large group such as the 2-chloro-4-(thiazol-5-yl)phenyl of the FRAX597 inhibitor is present. Based on this

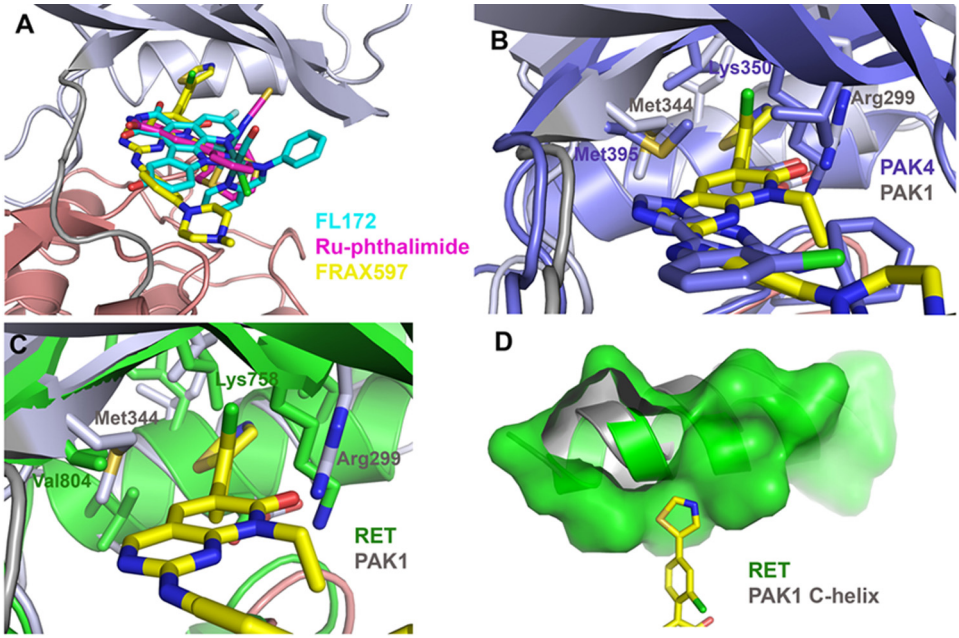

FIGURE 4. **Structural basis for FRAX597 potency and selectivity toward group I PAKs.** *A*, superimposition of the co-crystal structures of PAK1 with FL172 (PDB ID 3FXZ), Ru-phthalimide (PDB ID 4DAW), and FRAX597. The protein chain is only displayed for the PAK1/FRAX597 structure for clarity. *B*, superimposed co-crystal structures of PAK4/CGP74514A (PDB ID 2CDZ) and PAK1/FRAX597 illustrating the difference in size of the back pocket between two kinases. PAK4 is shown in *blue*, and PAK1 is shown in *gray*. *C*, superimposed cocrystal structures of RET (PDB ID 2IVU) and PAK1 kinases showing that the thiazole ligand of FRAX597 is not optimally accommodated by the back pocket of RET (shown in "*green*"). *D*, surface view and cartoon representation of the RET and PAK1 demonstrating the difference in the size of the back pockets and position of C-helices. The RET surface and C-helix are outlined in *green* and the PAK1 C-helix in *gray*.

observation, it is not surprising that a 100 nM concentration of FRAX597 does not show detectable inhibition against PAK4, while the same compound concentration inhibits more than 80% of PAK1 activity (data not shown).

To test the hypothesis that the size and accessibility of the back cavity could be an important determinant for FRAX597 selectivity toward PAK1 we mutated the Val-342 in the back cavity into phenylalanine (V342F) and tyrosine (V342Y), with the expectation that the bulky side chains would sterically interfere with the thiazole of the 2-chloro-phenyl and reduce inhibition of PAK1 by FRAX597. As expected the V342F and V342Y PAK1 mutants were less sensitive to FRAX597 inhibition and displayed significantly higher IC_{50} values. When measured using the Kinase Glo Assay in the presence of 20 nM protein and 1 μM ATP, FRAX597 displayed an IC_{50} value of 48 nM against wild type PAK1, while IC_{50} values against the V342F and V342Y PAK1 mutants were higher than 3 μM and 2 μM, respectively (Fig. 3*D*). Importantly, the purified mutant proteins behaved similarly to the wild type protein during purification and displayed similar overall kinase activities as determined by *in vitro* kinases assays (not shown).

Finally, the finding that the accessibility of the back cavity is a critical determinant of FRAX597 selectivity is further demonstrated when the PAK1/FRAX597 structure is superimposed with the receptor tyrosine kinase RET (Rearranged During Transfection) (41). RET is one of the few receptor tyrosine kinases that are targeted by FRAX597 with similar potency as PAK1 (data not shown). This superimposition demonstrates that the small Val-804 gatekeeper residue in RET allows access to the back cavity, likely allowing the RET active site to accommodate the 2-chloro-4-(thiazol-5-yl)phenyl group of FRAX597 (Fig. 4*C*). However, the C helix of RET is rotated into the back cavity more than it is in PAK1, serving to further constrict the back of the pocket in RET relative to PAK1 (Fig. 4*D*). Although RET could accommodate the thiazole substituent of FRAX597, we hypothesize that larger substituents would not be accommodated in RET. Interestingly, out of three additional receptor tyrosine kinases inhibited by FRAX597 with similar potency as RET, two have small threonine residues as the gatekeeper residue (YES1 and CSF1R) while one has a medium sized isoleucine (TEK) (data not shown), suggesting that they also accommodate FRAX597 in a similar fashion as RET.

FRAX597 Inhibits Schwannoma Cell Proliferation in Vitro and Tumor Formation in Vivo—To assess if FRAX597 can inhibit proliferation of transformed Schwann cells, *Nf2*-null SC4 Schwann cells were treated with the inhibitor, and cell numbers were followed over a period of 96 h. As shown in Fig. 5*A*, FRAX597 treatment dramatically impaired cellular proliferation. Propidium iodide and FACS analysis confirmed cell cycle arrest in G1, as evidenced by accumulation of FRAX597-treated cells in G1 phase (74% *versus* 50% in control-treated cells) and decrease in the fraction of cells in S phase (12% *versus* 27% in control) and G2/M phase (11% *versus* 22% in control). The absence of a sub-G1 population in treated cells suggests that FRAX597 does not impact cell viability (Fig. 5*B*). To determine if FRAX597 can inhibit tumor growth *in vivo*, we employed an orthotopic model of NF2 that recapitulates the tumor microenvironment of schwannomas, by injection of luciferase-tagged NF2-null schwannoma cells into a myelinated nerve (42, 43). Tumor progression was monitored twice weekly by bioluminescence imaging (BLI) and total flux counts were

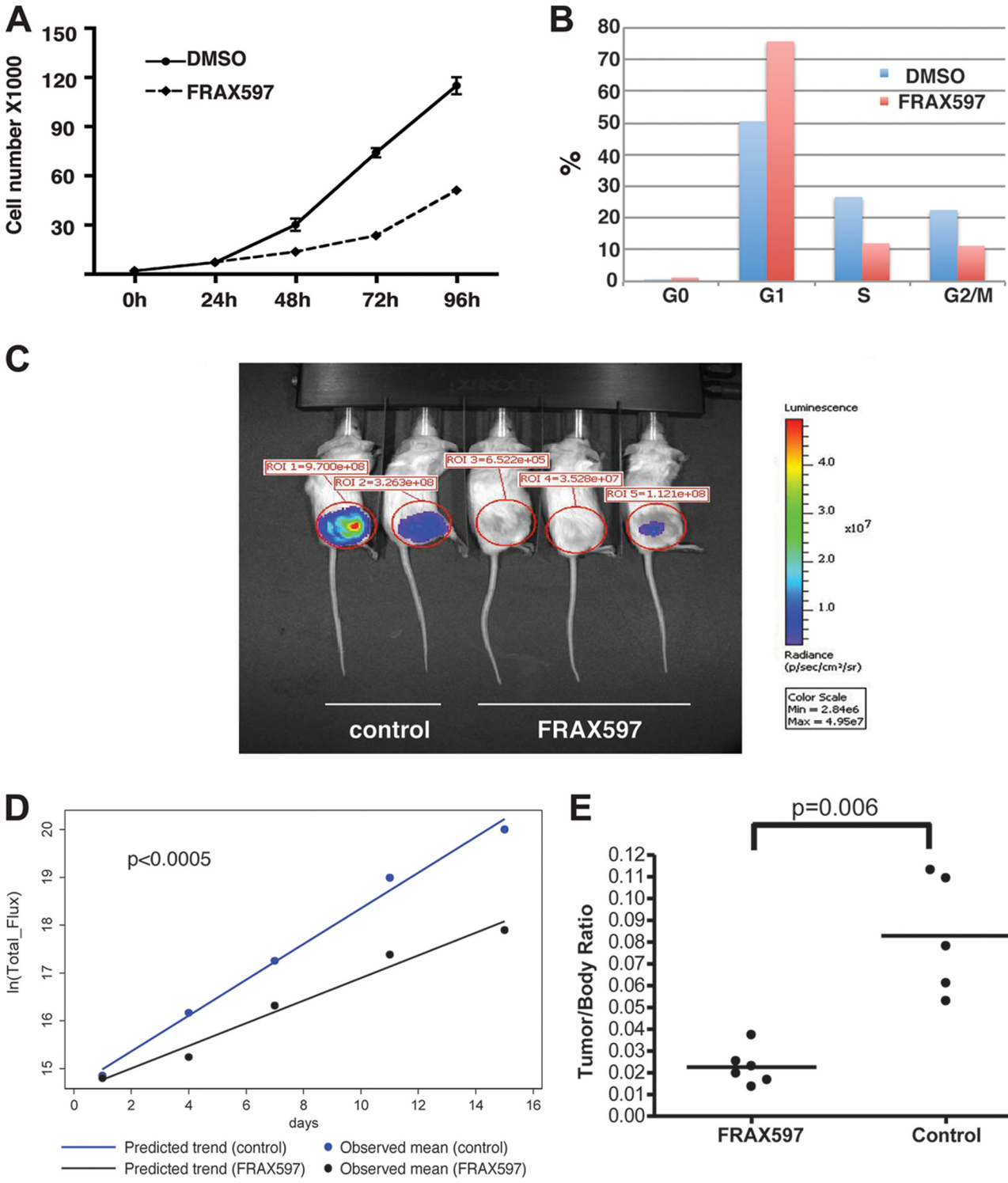

FIGURE 5. **FRAX597 inhibits tumor cells proliferation and tumor growth *in vivo*.** *A*, SC4 Nf2-null cells were plated in triplicate wells and treated with FRAX597 (1 μM) or DMSO control daily for 4 days, and cell numbers were scored daily. The experiment shown is representative of three independent experiments. *B*, percentage of treated SC4 cells in different phases of the cell cycle. The DNA content of treated SC4 cells was determined by staining with PI and analysis by FACS. The experiment shown is representative of three independent experiments. *C*, representative images from bioluminescence imaging (BLI) of mice carrying orthotopic tumors treated with FRAX597 (100 mg/kg) or vehicle control at day 14 of treatment. NOD/SCID mice were injected intraneurally with 5×10^4 SC4/pLuc-mCherry cells and were enrolled into treatment after 10 days. Mice were treated daily for 14 days and imaged every 3 days to follow tumor development. *D*, quantitative analysis of the flux reading from treated cohorts. A mixed-effect model analysis indicated that the speed of tumor growth in treatment group is significantly slower than that in control group ($p = 0.0002$). *E*, distribution of tumor/body weight ratios in the cohorts treated with FRAX597 or vehicle control. The results of *t* test with equal variances show that FRAX-A group has significant lower average tumor weight ratio than that observed in control group ($p = 0.0001$). For the *in vivo* experiments the $n = 6$ in each cohort, experiments repeated three times.

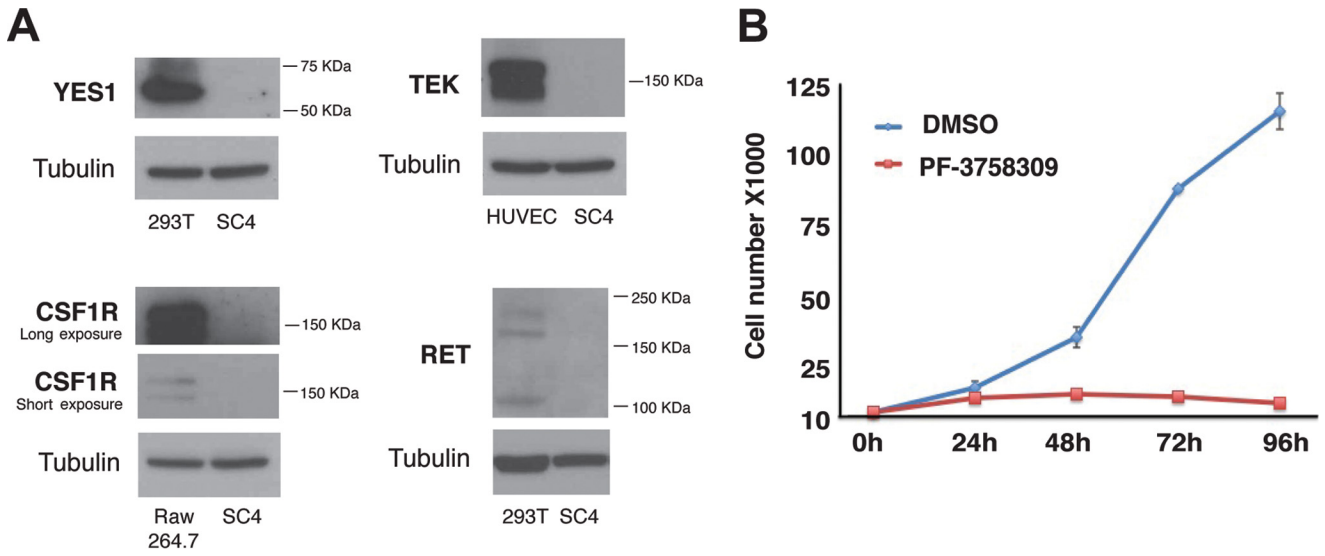

FIGURE 6. **Inhibition of group I PAKs mediates FRAX597 inhibition of SC4 cells.** *A*, Western blot analysis of Yes1, TEK, CSF1R and Ret expression in SC4 cells compared with relevant positive control cells. Tubulin was used as a loading control. *B*, SC4 Nf2-null cells were plated in triplicate wells and treated with PF3758309 (1 μM) or DMSO control daily for 4 days, and cell numbers were scored daily. The experiment shown is representative of three independent experiments.

recorded for each animal. Ten days postinjection, similar flux readings for all animals were validated, and animals were enrolled randomly into control (vehicle only) or drug-treated cohorts (100 mg/kg, oral, once daily) for a period of 14 days. Analysis of the flux reading for the animals in the two cohorts demonstrated a significantly slower tumor growth rate in FRAX597-treated mice compared with control mice (Fig. 5*B*). After 14 days of treatment the animals were sacrificed and the tumors excised and weighed. FRAX597-treated cohort showed significantly lower average tumor weight compared with the control cohort (0.55gr *versus* 1.87gr, $p = 0.0001$). Taken together, these data demonstrate that FRAX597 has a significant anti-proliferative activity against *Nf2*-null Schwann cells *in vitro* and anti-tumor activity *in vivo*.

The Inhibition of Group I PAKs Mediates FRAX597 Inhibition of Schwannoma Cell Proliferation—To further characterize the targets through which FRAX597 inhibits the proliferation of *NF2*-null Schwann cells, we assessed the expression level of the other kinases toward which FRAX597 displayed a significant inhibitory capacity (YES1, TEK, CSF1R, and RET) in SC4 cells. We find these kinases are not expressed, or below levels of detection, in these cells (Fig. 6*A*), thus suggesting it is unlikely the effects of FRAX597 on SC4 cell growth are mediated through inhibition of these targets.

In addition, we employed another PAK inhibitor from Pfizer (PF-3758309), which potently suppresses both group I (PAK1, PAK2, and PAK3) and II (PAK4, PAK5, and PAK6) PAKs (44). Importantly, while both FRAX597 and PF-3758309 display some limited off-target effects on other kinases, these off-target effects are largely non-overlapping (45). In assessing the effects on SC4 cell growth, PF-3758309 treatment resulted in a similar inhibition of cell proliferation as exhibited by FRAX597 treatment (Fig. 6*B*). These results suggest that the effects of FRAX597 seen in Nf2-null Schwann cells are mediated through inhibition of the group I PAKs.

DISCUSSION

The identification of FRAX597 as a potent inhibitor of group I PAKs has allowed us to assess the consequences of PAK inhibition on tumor development in an orthotopic model of NF2 that closely reflects the human disease. Consistent with our previous studies demonstrating that group I PAKs are critical effectors of merlin's tumor suppressive functions, we find that by inhibiting PAKs we are able to inhibit the proliferation of Nf2-null Schwann cells in culture and growth of NF2-associated schwannomas *in vivo*. While the possibility that part of the anti-tumor effects of FRAX597 can be attributed to targets other than the PAKs cannot be excluded, we find that other FRAX597 targets are not expressed in SC4 cells. Finally, treatment of SC4 cells with another PAK inhibitor (PF-3758309), which has off-target effects that are largely non-overlapping with FRAX597, recapitulates the effects of FRAX597 on SC4 cells. These combined findings strengthen the notion that the effects of FRAX597 inhibition are mediated through the inhibition of the group I PAKs.

Although relatively poorly conserved among different kinases, the back cavity of the ATP binding site is rarely targeted by kinase inhibitors. This cavity is typically hydrophobic and its accessibility depends on the size and position of the gatekeeper residue. For example, the BRAF and CDK2 kinases have small (Thr) and large (Phe) gatekeeper residues, respectively, allowing BRAF to have a larger cavity in this area creating what is known as a BRAF specificity pocket (46), while this region is essentially blocked off in CDK2 (47). In PAK1, the position of the Met-344 gatekeeper residue and the C-helix create a relatively large back cavity capable of accommodating the large 2-chloro-4-(thiazol-5-yl)phenyl moiety attached to the C6 position of the pyrido[2,3-d]pyrimidin-7-one ring system. Interestingly, some pyrido[2,3-d]pyrimidin-7-one derivatives were previously described as potent cyclin-dependent kinases (CDKs) inhibitors (47, 48). Some of them also contained a

methyl-piperazine phenylamino substituent at the C2 position of the same pyrido[2,3-d]pyrimidin-7-one ring system as FRAX597 (Fig. 2*A*). However, CDKs were found unable to accommodate large substituents at the C6 position (data not shown), consistent with the larger Phe gatekeeper residue in CDKs (49). Based on this observation, it is not surprising that FRAX597 exhibits no detectable potency against CDKs. The importance of the back pocket of the ATP binding site for PAK1 inhibition, and for inhibition by FRAX597 in particular, is further supported by the mutational sensitivity of Val-342 for inhibitor potency. This further highlights the importance of elaboration of the FRAX597 thiazole group for increasing PAK1 inhibitor potency and selectivity. In addition, elaboration of the methylpiperazine moiety on the opposite end of the FRAX597 inhibitor could provide additional opportunity to probe the protein substrate-binding site of PAK1.

Identification of this highly-selective group I PAK inhibitor and its ability to inhibit the proliferation of Nf2-null Schwann cells in culture and growth of NF2-associated schwannomas *in vivo* establish the group I PAKs as targets for the development of therapeutics. Determination of the PAK1/FRAX597 structure will guide further improvements of inhibitor potency and selectivity and provide opportunity to develop drugs for Neurofibromatosis type 2, a disease for which there are no approved therapeutics.

REFERENCES

1. Zhao, Z. S., and Manser, E. (2012) PAK family kinases: Physiological roles and regulation. *Cell Logist.* **2,** 59–68
2. Ridley, A. J., Paterson, H. F., Johnston, C. L., Diekmann, D., and Hall, A. (1992) The small GTP-binding protein rac regulates growth factor-induced membrane ruffling. *Cell* **70,** 401–410
3. Nobes, C. D., and Hall, A. (1995) Rho, rac, and cdc42 GTPases regulate the assembly of multimolecular focal complexes associated with actin stress fibers, lamellipodia, and filopodia. *Cell* **81,** 53–62
4. Ye, D. Z., and Field, J. (2012) PAK signaling in cancer. *Cell Logist* **2,** 105–116
5. Molli, P. R., Li, D. Q., Murray, B. W., Rayala, S. K., and Kumar, R. (2009) PAK signaling in oncogenesis. *Oncogene* **28,** 2545–2555
6. Dummler, B., Ohshiro, K., Kumar, R., and Field, J. (2009) Pak protein kinases and their role in cancer. *Cancer Metastasis Rev.* **28,** 51–63
7. Balasenthil, S., Sahin, A. A., Barnes, C. J., Wang, R. A., Pestell, R. G., Vadlamudi, R. K., and Kumar, R. (2004) p21-activated kinase-1 signaling mediates cyclin D1 expression in mammary epithelial and cancer cells. *J. Biol. Chem.* **279,** 1422–1428
8. Ong, C. C., Jubb, A. M., Haverty, P. M., Zhou, W., Tran, V., Truong, T., Turley, H., O'Brien, T., Vucic, D., Harris, A. L., Belvin, M., Friedman, L. S., Blackwood, E. M., Koeppen, H., and Hoeflich, K. P. (2011) Targeting p21-activated kinase 1 (PAK1) to induce apoptosis of tumor cells. *Proc. Natl. Acad. Sci. U.S.A.* **108,** 7177–7182
9. Wang, R. A., Zhang, H., Balasenthil, S., Medina, D., and Kumar, R. (2006) PAK1 hyperactivation is sufficient for mammary gland tumor formation. *Oncogene* **25,** 2931–2936
10. Vadlamudi, R. K., Adam, L., Wang, R. A., Mandal, M., Nguyen, D., Sahin, A., Chernoff, J., Hung, M. C., and Kumar, R. (2000) Regulatable expression of p21-activated kinase-1 promotes anchorage-independent growth and abnormal organization of mitotic spindles in human epithelial breast cancer cells. *J. Biol. Chem.* **275,** 36238–36244
11. Shrestha, Y., Schafer, E. J., Boehm, J. S., Thomas, S. R., He, F., Du, J., Wang, S., Barretina, J., Weir, B. A., Zhao, J. J., Polyak, K., Golub, T. R., Beroukhim, R., and Hahn, W. C. (2011) Pak1 is a breast cancer oncogene that coordinately activates MAPK and MET signaling. *Oncogene* **31,** 3397–3408
12. Adam, L., Vadlamudi, R., Mandal, M., Chernoff, J., and Kumar, R. (2000) Regulation of microfilament reorganization and invasiveness of breast cancer cells by kinase dead p21-activated kinase-1. *J. Biol. Chem.* **275,** 12041–12050
13. Adam, L., Vadlamudi, R., Kondapaka, S. B., Chernoff, J., Mendelsohn, J., and Kumar, R. (1998) Heregulin regulates cytoskeletal reorganization and cell migration through the p21-activated kinase-1 via phosphatidylinositol-3 kinase. *J. Biol. Chem.* **273,** 28238–28246
14. Li, Q., Mullins, S. R., Sloane, B. F., and Mattingly, R. R. (2008) p21-Activated kinase 1 coordinates aberrant cell survival and pericellular proteolysis in a three-dimensional culture model for premalignant progression of human breast cancer. *Neoplasia* **10,** 314–329
15. Arias-Romero, L. E., Villamar-Cruz, O., Huang, M., Hoeflich, K. P., and Chernoff, J. (2013) Pak1 kinase links ErbB2 to β-catenin in transformation of breast epithelial cells. *Cancer Res.* **73,** 3671–3682
16. Gerber, P. A., Antal, A. S., Neumann, N. J., Homey, B., Matuschek, C., Peiper, M., Budach, W., and Bölke, E. (2009) Neurofibromatosis. *Eur. J. Med. Res.* **14,** 102–105
17. Tang, Y., Marwaha, S., Rutkowski, J. L., Tennekoon, G. I., Phillips, P. C., and Field, J. (1998) A role for Pak protein kinases in Schwann cell transformation. *Proc. Natl. Acad. Sci. U.S.A.* **95,** 5139–5144
18. Yang, F. C., Ingram, D. A., Chen, S., Hingtgen, C. M., Ratner, N., Monk, K. R., Clegg, T., White, H., Mead, L., Wenning, M. J., Williams, D. A., Kapur, R., Atkinson, S. J., and Clapp, D. W. (2003) Neurofibromin-deficient Schwann cells secrete a potent migratory stimulus for Nf1+/- mast cells. *J. Clin. Invest.* **112,** 1851–1861
19. Zhu, Y., Ghosh, P., Charnay, P., Burns, D. K., and Parada, L. F. (2002) Neurofibromas in NF1: Schwann cell origin and role of tumor environment. *Science* **296,** 920–922
20. Yang, F. C., Ingram, D. A., Chen, S., Zhu, Y., Yuan, J., Li, X., Yang, X., Knowles, S., Horn, W., Li, Y., Zhang, S., Yang, Y., Vakili, S. T., Yu, M., Burns, D., Robertson, K., Hutchins, G., Parada, L. F., and Clapp, D. W. (2008) Nf1-dependent tumors require a microenvironment containing $Nf1^{+/-}$ and c-kit-dependent bone marrow. *Cell* **135,** 437–448
21. McDaniel, A. S., Allen, J. D., Park, S. J., Jaffer, Z. M., Michels, E. G., Burgin, S. J., Chen, S., Bessler, W. K., Hofmann, C., Ingram, D. A., Chernoff, J., and Clapp, D. W. (2008) Pak1 regulates multiple c-Kit mediated Ras-MAPK gain-in-function phenotypes in $Nf1^{+/-}$ mast cells. *Blood* **112,** 4646–4654
22. Stamenkovic, I., and Yu, Q. (2010) Merlin, a "magic" linker between extracellular cues and intracellular signaling pathways that regulate cell motility, proliferation, and survival. *Curr. Protein Pept. Sci.* **11,** 471–484
23. Nakai, Y., Zheng, Y., MacCollin, M., and Ratner, N. (2006) Temporal control of Rac in Schwann cell-axon interaction is disrupted in NF2-mutant schwannoma cells. *J. Neurosci.* **26,** 3390–3395
24. Kaempchen, K., Mielke, K., Utermark, T., Langmesser, S., and Hanemann, C. O. (2003) Upregulation of the Rac1/JNK signaling pathway in primary human schwannoma cells. *Hum. Mol. Genet.* **12,** 1211–1221
25. Yi, C., Wilker, E. W., Yaffe, M. B., Stemmer-Rachamimov, A., and Kissil, J. L. (2008) Validation of the p21-activated kinases as targets for inhibition in neurofibromatosis type 2. *Cancer Res.* **68,** 7932–7937
26. Flaiz, C., Kaempchen, K., Matthies, C., and Hanemann, C. O. (2007) Actin-rich protrusions and nonlocalized GTPase activation in Merlin-deficient schwannomas. *J. Neuropathol. Exp. Neurol.* **66,** 608–616
27. Wilkes, M. C., Repellin, C. E., Hong, M., Bracamonte, M., Penheiter, S. G., Borg, J. P., and Leof, E. B. (2009) Erbin and the NF2 tumor suppressor Merlin cooperatively regulate cell-type-specific activation of PAK2 by TGF-β. *Dev Cell* **16,** 433–444
28. Xiao, G. H., Gallagher, R., Shetler, J., Skele, K., Altomare, D. A., Pestell, R. G., Jhanwar, S., and Testa, J. R. (2005) The NF2 tumor suppressor gene product, merlin, inhibits cell proliferation and cell cycle progression by repressing cyclin D1 expression. *Mol. Cell Biol.* **25,** 2384–2394
29. Hirokawa, Y., Tikoo, A., Huynh, J., Utermark, T., Hanemann, C. O., Giovannini, M., Xiao, G. H., Testa, J. R., Wood, J., and Maruta, H. (2004) A clue to the therapy of neurofibromatosis type 2: NF2/merlin is a PAK1 inhibitor. *Cancer J.* **10,** 20–26
30. Kissil, J. L., Wilker, E. W., Johnson, K. C., Eckman, M. S., Yaffe, M. B., and Jacks, T. (2003) Merlin, the product of the Nf2 tumor suppressor gene, is an inhibitor of the p21-activated kinase, Pak1. *Mol. Cell* **12,** 841–849
31. Morrison, H., Sperka, T., Manent, J., Giovannini, M., Ponta, H., and Her-

rlich, P. (2007) Merlin/neurofibromatosis type 2 suppresses growth by inhibiting the activation of Ras and Rac. *Cancer Res.* **67,** 520–527
32. Chow, H. Y., Stepanova, D., Koch, J., and Chernoff, J. (2010) p21-Activated kinases are required for transformation in a cell-based model of neurofibromatosis type 2. *PLoS One* **5,** e13791
33. Flaiz, C., Chernoff, J., Ammoun, S., Peterson, J. R., and Hanemann, C. O. (2009) PAK kinase regulates Rac GTPase and is a potential target in human schwannomas. *Exp. Neurol.* **218,** 137–144
34. Otwinowski, Z., and Miner, T. (1997) *Methods in Enzymology*, pp. 307–326, Elsevier Academic Press, San Diego
35. Maksimoska, J., Feng, L., Harms, K., Yi, C., Kissil, J., Marmorstein, R., and Meggers, E. (2008) Targeting large kinase active site with rigid, bulky, octahedral ruthenium complexes. *J. Am. Chem. Soc.* **130,** 15764–15765
36. Murshudov, G. N., Vagin, A. A., and Dodson, E. J. (1997) Refinement of macromolecular structures by the maximum-likelihood method. *Acta Crystallogr D. Biol. Crystallogr* **53,** 240–255
37. Emsley, P., and Cowtan, K. (2004) Coot: model-building tools for molecular graphics. *Acta Crystallogr D. Biol. Crystallogr* **60,** 2126–2132
38. Maksimoska, J., Feng, L., Harms, K., Yi, C., Kissil, J., Marmorstein, R., and Meggers, E. (2008) Targeting large kinase active site with rigid, bulky octahedral ruthenium complexes. *J. Am. Chem. Soc.* **130,** 15764–15765
39. Blanck, S., Maksimoska, J., Baumeister, J., Harms, K., Marmorstein, R., and Meggers, E. (2012) The art of filling protein pockets efficiently with octahedral metal complexes. *Angew Chem. Int. Ed. Engl.* **51,** 5244–5246
40. Eswaran, J., Lee, W. H., Debreczeni, J. E., Filippakopoulos, P., Turnbull, A., Fedorov, O., Deacon, S. W., Peterson, J. R., and Knapp, S. (2007) Crystal Structures of the p21-activated kinases PAK4, PAK5, and PAK6 reveal catalytic domain plasticity of active group II PAKs. *Structure* **15,** 201–213
41. Knowles, P. P., Murray-Rust, J., Kjaer, S., Scott, R. P., Hanrahan, S., Santoro, M., Ibáñez, C. F., and McDonald, N. Q. (2006) Structure and chemical inhibition of the RET tyrosine kinase domain. *J. Biol. Chem.* **281,** 33577–33587
42. Saydam, O., Ozdener, G. B., Senol, O., Mizrak, A., Prabhakar, S., Stemmer-Rachamimov, A. O., Breakefield, X. O., and Brenner, G. J. (2011) A novel imaging-compatible sciatic nerve schwannoma model. *J. Neurosci. Methods* **195,** 75–77
43. Wong, H. K., Lahdenranta, J., Kamoun, W. S., Chan, A. W., McClatchey, A. I., Plotkin, S. R., Jain, R. K., and di Tomaso, E. (2010) Anti-vascular endothelial growth factor therapies as a novel therapeutic approach to treating neurofibromatosis-related tumors. *Cancer Res.* **70,** 3483–3493
44. Murray, B. W., Guo, C., Piraino, J., Westwick, J. K., Zhang, C., Lamerdin, J., Dagostino, E., Knighton, D., Loi, C. M., Zager, M., Kraynov, E., Popoff, I., Christensen, J. G., Martinez, R., Kephart, S. E., Marakovits, J., Karlicek, S., Bergqvist, S., and Smeal, T. (2010) Small-molecule p21-activated kinase inhibitor PF-3758309 is a potent inhibitor of oncogenic signaling and tumor growth. *Proc. Natl. Acad. Sci. U.S.A.* **107,** 9446–9451
45. Chow, H. Y., Jubb, A. M., Koch, J. N., Jaffer, Z. M., Stepanova, D., Campbell, D. A., Duron, S. G., O'Farrell, M., Cai, K. Q., Klein-Szanto, A. J., Gutkind, J. S., Hoeflich, K. P., and Chernoff, J. (2012) p21-Activated kinase 1 is required for efficient tumor formation and progression in a Ras-mediated skin cancer model. *Cancer Res.* **72,** 5966–5975
46. Zuccotto, F., Ardini, E., Casale, E., and Angiolini, M. (2010) Through the "gatekeeper door": exploiting the active kinase conformation. *J. Med. Chem.* **53,** 2681–2694
47. Barvian, M., Boschelli, D. H., Cossrow, J., Dobrusin, E., Fattaey, A., Fritsch, A., Fry, D., Harvey, P., Keller, P., Garrett, M., La, F., Leopold, W., McNamara, D., Quin, M., Trumpp-Kallmeyer, S., Toogood, P., Wu, Z., and Zhang, E. (2000) Pyrido[2,3-d]pyrimidin-7-one inhibitors of cyclin-dependent kinases. *J. Med. Chem.* **43,** 4606–4616
48. VanderWel, S. N., Harvey, P. J., McNamara, D. J., Repine, J. T., Keller, P. R., Quin, J., 3rd, Booth, R. J., Elliott, W. L., Dobrusin, E. M., Fry, D. W., and Toogood, P. L. (2005) Pyrido[2,3-d]pyrimidin-7-ones as specific inhibitors of cyclin-dependent kinase 4. *J. Med. Chem.* **48,** 2371–2387
49. Lu, H., and Schulze-Gahmen, U. (2006) Toward understanding the structural basis of cyclin-dependent kinase 6 specific inhibition. *J. Med. Chem.* **49,** 3826–3831

FRAX597, a Small Molecule Inhibitor of the p21-activated Kinases, Inhibits Tumorigenesis of Neurofibromatosis Type 2 (NF2)-associated Schwannomas

Silvia Licciulli, Jasna Maksimoska, Chun Zhou, Scott Troutman, Smitha Kota, Qin Liu, Sergio Duron, David Campbell, Jonathan Chernoff, Jeffrey Field, Ronen Marmorstein and Joseph L. Kissil

J. Biol. Chem. 2013, 288:29105-29114.
doi: 10.1074/jbc.M113.510933 originally published online August 19, 2013
